P-ISSN 2586-9000
E-ISSN 2586-9027
Homepage : https://tci-thaijo.org/index.php/SciTechAsia
Science & Technology Asia
Vol.29 No.1 January - March 2024
Page: [160-181]
Original research article

Next Generation Heffron-Phillips Model for Damping Power System Oscillations based on a Novel Meta-Heuristic Snake Optimization Algorithm

Niharika Agrawal[1,*], Faheem Ahmed Khan[1], Sheila Mahapatra[2]

[1]*Department of Electrical and Electronics Engineering, Ghousia College of Engineering, Ramanagaram 562159, India*
[2]*Department of Electrical and Electronics Engineering, Alliance University, Karnataka 562106, India*

Received 3 June 2023; Received in revised form 5 December 2023
Accepted 12 January 2024; Available online 31 March 2024

ABSTRACT

Low-Frequency Oscillations (LFO) created due to various disturbances affect the integrity, security, efficiency, and safety of the power system. The traditional Heffron-Phillips (HP) Model of a power system has 6-K-Constants and the state vector is composed of only four state variables. In the present work, a higher-order Synchronous Machine Model 1.1 is used to develop the next-generation HP Model called an Advanced Heffron-Phillips Model (AHPM). There are now 5 state variables and 10 K-Constants including the dynamics of d and q-axis internal voltages. A novel meta-heuristic snake optimization algorithm (SOA) with the key features of exploration and exploitation is used for optimizing the parameters of PSS, TCSC, and Coordinated PSS and TCSC, and the results are compared. The coordinated model based on AHPM produced excellent stability results. The system oscillations died out fastest, with a settling time of less than 2 seconds, and a damping ratio as high as 99.30% is achieved with the coordinated model. Together with the graphical responses, the dominant eigenvalues are mentioned to highlight this notable shift in performance. The system's power transfer capacity is also improved along with stability. The integration of renewables into the grid creates new stability issues and challenges. This AHPM based on SOA is capable of meeting these challenges. The power grid with AHPM is more efficient, robust, secure, and safe against unpredictable operating conditions with renewables.

Keywords: Algorithm; Model; Damping; Objective function; Oscillations; Stability

***Corresponding author:** niharika.svits@gmail.com **doi:** 10.14456/scitechasia.2024.12

1. Introduction

Power System oscillations were observed in the Great Britain Power System Network in the 1980s due to the relatively heavy loading of transmission lines with a frequency of 0.5 Hz. In 1984 these oscillations were seen in the Taiwan Power Network which transferred large amounts of power to HV transmission lines. Due to the loss of a 500-kV line in the North American WSCC network, there were observed oscillations whose range of frequency was between 0.2 Hz and 0.3 Hz. The oscillations can also be caused due to severe faults or tripping of some transmission lines, loss of a generator, or when the network is exposed to small/large disturbances, and as such these oscillations belong to large-signal or small signal stability problems. The power system may completely collapse if these oscillations are not managed. The Small Signal Stability (SSS) studies are done for damping Low Frequency Oscillations (LFO). The SSS is the fundamental and essential for the system's successful operation. Due to the power system being complex and having non-linear characteristics the system's linearization is done for SSS studies with the HP Model using Taylor's series expansion with the consideration of small perturbation [1, 2].

To dampen LFOs and enhance the stability characteristics of the system, a power system stabilizer (PSS) is incorporated into the network. But because the traditional PSS is predicated on set parameters, its performance is deemed insufficient when the operating environment shifts. PSS is then designed with a lead-lag structure with parameters tuned by different optimization algorithms. It is found that the PSS is effective at attenuating the local oscillation modes (frequency range 0.7 to 1.5 Hz). There are interarea modes of oscillations with a frequency range of 0.1 to 0.7 Hz. Thus, it is determined that the system needs better and more controllers. The advantages of utilizing FACTS, or Flexible AC Transmission System controllers are widely recognized. One type of series FACTS device that is used to increase the capacity of power flow transfer is the Thyristor Controlled Series Capacitor (TCSC). It also provides adequate damping for inter-area modes of oscillations. The TCSC device is more effective in the areas of power flow control and damping performance than the shunt-connected controllers [3, 4]. Hence this device is included in the system with PSS. The TCSC controllers for stability are designed using a conventional lead-lag structure as it is easy to tune and flexible. The PSS and TCSC devices are coordinated to have better damping characteristics and stability and to provide damping control to both the oscillation modes (local, and inter-area). Proper coordination between the two devices is necessary to avoid destabilizing interactions [5].

The key component of the power system is the synchronous machine (SM). It is shown by the Park Model's d and q-axes. The SM has three-phase armature windings on the stator which are the 'a' winding, the 'b' winding and the 'c' winding. There are four (4) windings on the rotor which are 'f', 'h', 'g', and 'k'. The field winding is 'f' winding. The 'h', 'g', and 'k' are the damper windings. The 'h' damper coil is on the d-axis and the two damper coils which are the 'g' coil and the 'k' coil are on the q-axis. Several approximations of the (Synchronous Generator) SG Model are done for performing simulation and for the analysis of stability. The work is done on the classical model (CM) which is the most simple and basic model of SM. Studies on first swing transient stability that use brief study periods—one second or less—benefit from the use of this CM. This is a second order model and it is governed by only 2 (two) state variables which are (δ, ω). In this CM there is no incorporation of exciter dynamics. Transients of stator and network are neglected in CM [6].

The Heffron-Phillips (HP) model of the power system is used to investigate the stability of SM under minor perturbations.

The PSS is included to provide the additional damping torque required for stability. Six K-Constants, which reflect the system dynamics, serve as the foundation for this model. The SM/SG Model 1.0 is used for the development of the HP model which considered only the field winding 'f' of the machine. The assumption considered is a sufficiently smaller value of the term Tq0' (q-axis transient time constant). Therefore, the damper coil '1q' on the q-axis dynamics is not considered. SM Model 1.0 is a 3rd(third) order SM Model. The SM Model 1.0 is most suitable where the time factor is most critical and important e.g., for operational planning studies for the selective contingency analysis.

This SM Model 1.0 is generally known as the one-axis (1-axis) flux decay model. The dynamics of d-axis internal voltage are not considered in the HP Model based on SG Model 1.0 [7]. This HP Model based on SM Model 1.0 is called here as an Old Heffron-Phillips Model (OHPM).

In order to construct the supplementary damping controller and its installation control channel inside the SSSC, the authors in [8] propose a meta-heuristic optimization technique. This method involves installing a damping controller to increase maximum stability and resistance under various operating settings by examining two control channels: phase and magnitude. A control channel that works well has been chosen. Using the sum of weighted coefficients approach, the optimization method considers more than one objective function. In [9] for improving the power system stability, the authors propose a type-2 fuzzy lead-lag (T2FLL) controller structure for PSSs and damping controllers based on FACTS. Using a hybrid adaptive differential evolution and pattern search algorithm (hADE-PS) approach, the recommended controller's values are optimized. First, a lead-lag (LL)-structured FACTS and PSS controller-equipped single-machine infinite-bus (SMIB) system is examined, and the superiority of the hADE-PS approach over the original Differential Evolution (DE), Genetic Algorithm (GA), and PSO is established. The study in [10] suggests a novel approach that considers time delays when simultaneously adjusting the FACTS controller and PSS. The suggested controller's design is represented as an optimization task. The Grasshopper Optimization Algorithm (GOA) is implemented to tune/optimize the controller's parameters. The effectiveness of the proposed controller is assessed in multi-machine power systems and single-machine infinite bus systems with different disturbances. The work has all been completed using a multimachine system or the Old Heffron-Phillips Model. The SM Model 1.0 is used in all these research works.

In the proposed research work a higher order SM 1.1 Model is implemented for providing damping to the power system. The 1.1 Model considers one rotor circuit on the d–axis and the other rotor circuit on the q–axis (damper coil/winding '1q'). This SM Model 1.1 represents the system in more detail, is better for stability analysis/studies, and is a fourth-order model. It is easy to incorporate the dynamics of an exciter in Model 1.1. SM Model 1.1 is also called a 2-axis model in studies. The damping controller based on SM Model 1.1 is called here as an Advanced Heffron-Phillips Model- AHPM. It has been concluded in [11] that SM Model 1.1 is more suitable for the analysis of transient stability.

Various algorithms, tools, and techniques have been implemented for tuning the parameters of PSS like the Whale Optimization algorithm [12], Sea-Horse optimizer [13], Golden Jackal [14], Equilibrium Optimizer [15], DE [16], Machine Learning based PSS [17], Improved GA [18], Dingo [19], Tunicate Swarm [20]. Table 1 describes the challenges and features of different algorithms. These algorithms can improve the performance of the system; however, according to Free Lunch Theory (FLT) further improvement is possible

despite having promising results with the previous algorithms. The FLT also states that no Meta-Heuristic Algorithm (MHA) is able to give the solution to all types of optimization problems. The FLT and scope for further and continuous improvement motivated the authors of this present work to develop a novel algorithm and higher order SM Model 1.1 for the design of a robust power system.

In the present work, a recently proposed MHA in Knowledge-Based Systems in 2022 called the Snake Optimization Algorithm (SOA) is implemented for tuning the different parameters of various controllers. It is an excellent algorithm for solving scientific and engineering problems. It is inspired by the unique mating behaviour of snakes and has various benefits; it is easy to implement, is flexible, and suitable for use as a black box. It avoids getting trapped in local optima and is able to find the near-optimal /optimal solutions.

With the inclusion of dynamics of d-axis internal voltage and excellent SOA, this AHPM is capable of meeting the grid integration issues with renewables. The renewables contribute to unforeseen conditions and transient stability issues in the system. There is a reduction in stored kinetic energy with renewables. In addition to meeting the stability challenges of grid integration with renewables, this AHPM with SOA can operate in a range of operating conditions.

Table 1. Challenge and features.

Author [citation]	Optimization Algorithms/ Methodology	Features	Challenges
Jokarzadeh et al. [16]	DE	The response speed is enhanced amidst oscillations. Suitable supplementary control loop based on LQR is suggested.	It does not test the entire loading situation.
Morsali et al. [21]	IPSO	Highest dynamic performance is offered related to oscillations, settling time, decreased maximum peak, minimized ITSE, and enhanced minimum damping ratio. It is robust under the large uncertainty scenarios.	It does not test the entire loading situations.
Morsali et al. [22]	MGSO	It is stable and robust under the specified variations. It stabilizes power deviations and frequency of the area frequency in a better way.	It does not guarantee the best possible response under all power system operating conditions.
Salgotra and Pan [23]	Frequency-response matching technique	It enhances the ISE and the peak overall. Better step responses are offered with appreciable damping.	The robustness is not enhanced in a broad range of operating conditions.
Martins et al. [24]	PSO	It optimizes the parameters without considering the supplementary damping controller count. The damping levels of low-frequency oscillation modes are enhanced.	It takes more time for the simulations.
Zare et al. [25]	IPSO	It is robust and performs well in the uncertainty conditions. Greater dynamic performance is produced with time -domain characteristics of the system.	The utilization of AGC alone can ultimately lead to system instability.
Bakhshi et al. [26]	LFDC	The transient stability linked with the power systems is enhanced. Only the easily available local signals are used.	In some cases, it limits from multiple problems like delays and communication infrastructure failures.
Nie et al. [27]	ITAE	It provides faster convergence. The oscillations associated with the evaluated power systems are suppressed.	It does not coordinate the optimizing and designing of WADCs with time-changing delay and probabilistic techniques.

Electric Vehicles (EVs) have significant impacts on the power system during their charging and discharging operations. The EV can be considered as a load disturbance for oscillations [28, 29].

The contributions of the research paper are as follows:

1. The complexity of today's power networks underscores the need for advanced identification techniques. It should go without saying that more precise modelling leads to more precise controller designs and acceptable results. A higher-order, detailed SM Model 1.1 is used to create an effective damping controller for stability improvement.
2. Three steps comprise the research associated with mathematical modelling

which are the model construction, behaviour analysis, and model evaluation. All of the crucial parameters for some behaviours that are explained by differential equations must be included in the mathematical model. An effective mathematical model encompasses all of the study objectives and describes the behaviour of the original. This AHPM satisfies all these requirements.

3. The best system representation for identification, simulation and stability investigations is thought to be the state space representation. This is created with PSS, TCSC, CPT for both OHPM and AHPM. This representation is also the basis for the eigenvalue analysis.

4. There is less assumption and negligence of parameters.

5. A novel MHA SOA having the key features of exploration and exploitation is used. It has been tested and checked with different benchmark functions and statistical parameters.

6. There is a 5 by 5 state matrix instead of the earlier 4 by 4 state matrix of the system.

7. There are 10 K-Constants in AHPM instead of the 6 K-Constants in OHPM.

8. The dynamics of d-axis internal voltage are not neglected.

9. A robust and secure system is designed with this SM Model 1.1 and SOA.

10. The AHPM is capable of meeting the stability issues with renewables.

2. Methodology

2.1 Power system mathematical modelling

Various equations governing the dynamics of the exciters, generator, and control elements are involved in developing the OHPM. The other equations representing the network relations are the stator, rotor winding equations, the torque and rotor equations. Fig.1 represents the One Machine Infinite Bus System (OMIBS) schematic diagram with PSS, TCSC, and Coordinated PSS and TCSC(CPT). The Automatic Voltage Regulator (AVR) is added to the power system to control the excitation voltage. AVR with high gain and fast action improved the synchronizing torque however it was unable to deliver the required damping torque.

The PSS is added for the required damping torque. Due to a perturbance, there is a change in the generator's electromagnetic torque which is divided into two parts: the damping torque and the synchronizing torque. These two torques are essential for the system's stability. The PSS and TCSC are added to provide damping to local and interarea modes of oscillation. The two devices can be coordinated and the model is called the Coordinated PSS and TCSC Model. The parameters of all the models should be carefully tuned. Improper tuning may lead to destabilizing interactions.

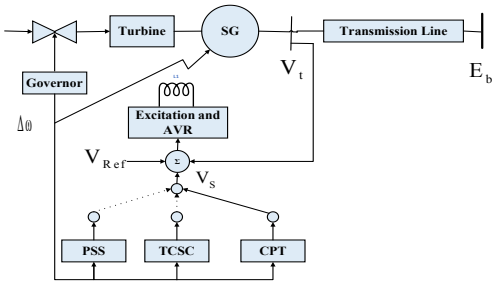

Fig. 1. The OMIBS.

2.2 Old Heffron-Phillips Model (OHPM)

This model, which has been used to analyse the system's stability, is based on the third order model of SG. The excitation control effect on the SM stability is explained by F.P. DeMello and C. Concordia. The OHPM based on 6 K-Constants is depicted in Fig. 2.

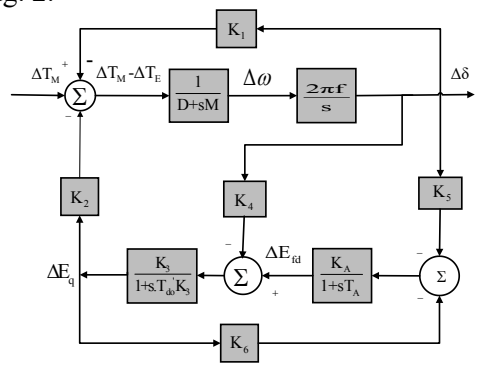

Fig. 2. The OHPM.

This model is based on 6 K-Constants known as Heffron-Phillips Constants given by:

$$K_1 = \frac{\partial P_E}{\partial \delta}, K_2 = \frac{\partial P_E}{\partial E'_q}, K_3 = \frac{\partial E_q}{\partial E'_q},$$
$$K_4 = \frac{\partial E_q}{\partial \delta}, K_5 = \frac{\partial V_t}{\partial \delta}, K_6 = \frac{\partial V_t}{\partial E'_q}.$$

The detailed expansion of these constants is

$$K_1 = \frac{E_b E_{q0} \cos\delta_0}{\left(x_e + x_q\right)} + \frac{\left(x_q - x'_d\right)}{\left(x_e + x'_d\right)} E_b i_{q0} \sin\delta_0, \quad (2.1)$$

$$K_2 = \frac{\left(x_e + x_q\right)}{\left(x_e + x'_d\right)} i_{q0} = \frac{E_b \sin\delta_0}{\left(x_e + x'_d\right)}, \quad (2.2)$$

$$K_3 = \frac{\left(x_e + x'_d\right)}{\left(x_d + x_e\right)}, \quad (2.3)$$

$$K_4 = \frac{\left(x_d + x'_d\right)}{\left(x_d + x_e\right)} E_b \sin\delta_0, \quad (2.4)$$

$$K_5 = \frac{-x_q v_{d0} E_b \cos\delta_0}{\left(x_e + x_q\right) v_{t0}} - \frac{x'_d v_{q0} E_b \sin\delta_0}{\left(x_e + x'_d\right) v_{t0}}, \quad (2.5)$$

$$K_6 = \frac{x_e}{\left(x_e + x'_d\right) v_{t0}} \left(\frac{v_{q0}}{V_{t0}}\right). \quad (2.6)$$

The OHPM has the following assumptions:

Disregarding the damper winding dynamics in the *d* and *q* axes.

The machine armature resistance is neglected.

The excitation system is represented by a single time constant system.

Consideration of a lossless network.

System's State-Space Model/Representation with OHPM.

$$\begin{bmatrix} \Delta\dot{\delta} \\ \Delta\dot{\omega}_m \\ \Delta\dot{E}'_q \\ \Delta\dot{E}_{fd} \end{bmatrix} = \begin{bmatrix} 0 & \omega_B & 0 & 0 \\ -\frac{K_1}{2H} & -\frac{D}{2H} & -\frac{K_2}{2H} & 0 \\ -\frac{K_4}{T'_{d0}} & 0 & -\frac{1}{T'_{d0}K_3} & \frac{1}{T'_{d0}} \\ -\frac{K_A K_5}{T_A} & 0 & -\frac{K_A K_6}{T_A} & -\frac{1}{T_A} \end{bmatrix} \begin{bmatrix} \Delta\delta \\ \Delta\omega_m \\ \Delta E'_q \\ \Delta E_{fd} \end{bmatrix} + \begin{bmatrix} 0 \\ 0 \\ 0 \\ \frac{K_A}{T_A} \end{bmatrix} U,$$

where U is the control input signal.

2.3 SM Model 1.1 equations for AHPM

The fourth order model of SM is used here. The dynamics of the SM are given by these equations [31]:

$$\frac{d\delta}{dt} = \omega - \omega_s, \quad (2.7)$$

$$\frac{2H}{\omega_{sq}} \frac{d\omega}{dt} = T_M E'_q I_q - E'_d I_d - \left(X'_q - X'_d\right) I_d I_q - T_{FW}, \quad (2.8)$$

$$T'_{do} \frac{dE'_q}{dt} = -E'_q - (X_d - X'_d) I_d + E_{fd}, \quad (2.9)$$

$$T'_{qo} \frac{dE'_d}{dt} = -E'_d + (X_q - X'_q) I_q. \quad (2.10)$$

The explanation and nomenclature for various terms in the equations are given in [30, 35].

2.4 Linearization and 10 K-Constants for AHPM

The system model is linearized for the SSS analysis. The initial conditions are calculated for SSS analysis of the system [32]. The Power/Load flow solution gives the operating point. For obtaining the Real Power (P) and Reactive Power (Q), magnitude, and voltage angle the calculation of power flow in steady-state is done. These K-Constants are [Novel Contribution].

$$K_1 = \frac{\partial T_E}{\partial \delta}, K_2 = \frac{\partial T_E}{\partial E'_q}, K_3 = \frac{\partial T_e}{\partial E'_d}, K_4 = \frac{\partial E'_q}{\partial E_q},$$
$$K_5 = \frac{\partial E'_q}{\partial \delta}, K_6 = \frac{\partial E'_d}{\partial E_d}, K_7 = \frac{\partial E'_d}{\partial \delta}, K_8 = \frac{\partial E_{fd}}{\partial \delta},$$
$$K_9 = \frac{\partial E_{fd}}{\partial E'_q}, K_{10} = \frac{\partial E_{fd}}{\partial E'_d}.$$

The detailed expansion is:

$$K_1 = -\left[E'_{do} + ((x'_d - x'_q)i_{q0})\right]\frac{E_{d0}E_b \sin\delta_0}{x_e + x'_d} + \left[(x'_d - x'_q)i_{d0} + E'_{qo}\right]\frac{E_b \cos\delta_0}{x_e + x'_d}, \quad (2.11)$$

$$K_2 = -\left[E'_{d0} + ((x'_d - x'_q)\, i_{q0})\right]\frac{1}{x_e + x'_d} + E'_{q0}\frac{1}{x_e + x'_q} + i_{q0}, \quad (2.12)$$

$$K_3 = \left[i_{d0} + ((x'_d - x'_q)\, i_{d0})\right]\frac{1}{x_e + x'_q}, \quad (2.13)$$

$$K_4 = \frac{x_e + x'_d}{(x_e + x'_d) + (x_d - x'_d)}, \quad (2.14)$$

$$K_5 = (x_d - x'_d)\frac{E_b \sin\delta_0}{x_e + x'_d}, \quad (2.15)$$

$$K_6 = \frac{x_e + x'_q}{(x_e + x'_q) + (x_q - x'_q)}, \quad (2.16)$$

$$K_7 = -(x_q - x'_q)\frac{E_b \cos\delta_0}{x_e + x'_q}, \quad (2.17)$$

$$K_8 = \frac{V_{do}}{V_{t0}}\left(-E_b \cos\delta_0 + \frac{x_e E_b \cos\delta_0}{x_e + x'_d}\right), \quad (2.18)$$

$$K_9 = \frac{V_{q0}x_e}{V_{t0}}\frac{1}{x_e + x'_d}, \quad (2.19)$$

$$K_{10} = \frac{V_{d0}x_e}{V_{t0}}\frac{1}{x_e + x'_q}. \quad (2.20)$$

2.5 System equations with AHPM

The system equations are modified with 10 K-Constants [33]. Now the new equations for rotor angle, speed, internal voltages and field voltages are:

$$\Delta\dot{\delta} = \omega_B \Delta\omega_m, \quad (2.21)$$

$$\Delta\dot{\omega}_m = -\frac{D}{2H}\Delta\omega_m + \frac{1}{2H}\Delta T_m - \frac{K_1}{2H}\Delta\delta - \frac{K_2}{2H}\Delta E'_q - \frac{K_3}{2H}\Delta E'_d, \quad (2.22)$$

$$\Delta\dot{E}'_q = \frac{1}{T'_{d0}}\left(\Delta E_{fd} - K_5\Delta\delta - \frac{\Delta E'_q}{K_4}\right), \quad (2.23)$$

$$\Delta\dot{E}'_d = \frac{1}{T'_{q0}}\left(K_7\Delta\delta - \frac{\Delta E'_d}{K_6}\right), \quad (2.24)$$

$$\Delta\dot{E}_{fd} = -\frac{K_A K_8}{T_A}\Delta\delta - \frac{K_A K_9}{T_A}\Delta E'_q - \frac{K_A K_{10}}{T_A}\Delta E'_d + \frac{K_A}{T_A}\Delta V_R - \frac{1}{T_A}\Delta E_{fd}. \quad (2.25)$$

2.6 The OMIBS with PSS and Exciter

Fig.3 shows PSS installed in OMIBS. PSS is added to mitigate the problem of oscillations created due to negative torque produced by AVR. The PSS provides the required additional torque for damping without affecting the synchronising torque. An additional voltage stabilizing signal (V_s) is added as input signal to the AVR. This signal is generated by PSS whose input is rotor speed deviation ($\Delta\omega$). The different input signals to the PSS can be frequency, rotor speed, electrical power or some combination of these signals. The PSS Lead Lag structure (PSSLLS) is used here. It has a gain block, a washout block which acts as a high-pass filter and a two stage lead-lag compensator block to compensate for the phase lag between the two signals[34].

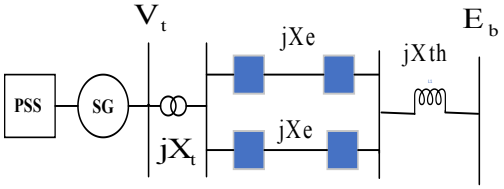

Fig. 3. The OMIBS with PSS.

2.7 The Advanced Heffron-Phillips Model (The AHPM)

In this model, the dynamics of the d-axis and q-axis both are considered. Fig. 4 shows this model. There are now 10 K-Constants governing the system dynamics. The state vector in AHPM is $\left[\Delta\delta \quad \Delta\omega \quad \Delta E'_q \quad \Delta E'_d \quad \Delta E_{fd}\right]^T$ and in OHPM it is $\left[\Delta\delta \quad \Delta\omega \quad \Delta E'_q \quad \Delta E_{fd}\right]^T$.

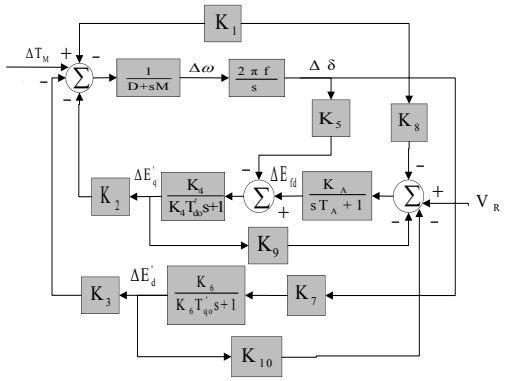

Fig. 4. The AHPM.

2.7.1 State Space Representation of the AHPM

$$\begin{bmatrix} \Delta\dot{\delta} \\ \Delta\dot{\omega}_m \\ \Delta\dot{E}'_q \\ \Delta\dot{E}'_d \\ \Delta\dot{E}_{fd} \end{bmatrix} = \begin{bmatrix} 0 & \omega_B & 0 & 0 & 0 \\ -\frac{K_1}{2H} & -\frac{D}{2H} & -\frac{K_2}{2H} & -\frac{K_3}{2H} & 0 \\ -\frac{K_5}{T'_{d0}} & 0 & -\frac{1}{T'_{do}K_4} & 0 & \frac{1}{T'_{d0}} \\ \frac{K_7}{T'_{q0}} & 0 & 0 & -\frac{1}{T'_{qo}K_6} & 0 \\ -\frac{K_A K_8}{T_A} & 0 & -\frac{K_A K_9}{T_A} & -\frac{K_A K_{10}}{T_A} & -\frac{1}{T_A} \end{bmatrix} \begin{bmatrix} \Delta\delta \\ \Delta\omega_m \\ \Delta E'_q \\ \Delta E'_d \\ \Delta E_{fd} \end{bmatrix}$$

$$+ \begin{bmatrix} 0 \\ \frac{1}{2H} \\ 0 \\ 0 \\ \frac{K_A}{T_A} \end{bmatrix} \begin{bmatrix} 0 & \Delta T_M & 0 & 0 & V_R \end{bmatrix}.$$

There are 5 state variables in this representation.

2.8 The OMIBS with TCSC

The TCSC controller is added with AHPM. The system reactance (X_e) is altered as a result of the TCSC being added as:

$$X_{Total} = X_e - X_{TCSC(\alpha)}.$$

The values of K-Constants also change due to the inclusion of TCSC. The system damping and power flow capacity can be effectively increased with the TCSC. The TCSC system consists of capacitor in parallel with a TCR. It provides variable compensation by changing the firing angle (α) of thyristors. The fundamental concept of TCSC is to provide variable compensation by changing the firing angle (α) of thyristors. The equation for the relation between reactance (X_{TCSC}) and firing angle (α) of TCSC is

$$X_{TCSC(\alpha)} = X_C - \frac{X_C^2}{(X_C - X_P)} \frac{(\sigma + \sin\sigma)}{\pi} + \frac{4X_C^2}{(X_C - X_P)} \frac{\cos^2(\sigma/2)}{(k^2-1)} \frac{[k\tan(k\sigma/2) - \tan(\sigma/2)]}{\pi}, \quad (2.26)$$

The equation showing the relation between electrical output power of a generator, angle and reactance of TCSC is.

$$P_t = \frac{E'_q V_B}{X'_{d\Sigma}} \sin\delta - \frac{V_B^2 \left(X_q - X'_d\right)}{2X'_{d\Sigma}X'_{q\Sigma}} \sin 2\delta. \quad (2.27)$$

Thus, by adjusting the firing angle, the electrical output power of SG/SM can be controlled and hence the damping capacity of the system.

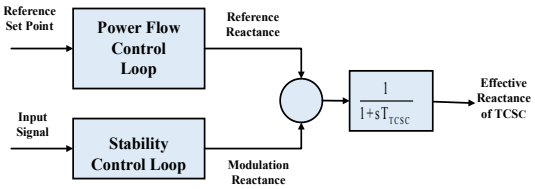

Fig. 5. The different loops for TCSC Model.

Fig. 5 shows the TCSC model which consists of two loops. The effective TCSC reactance is given by the equation.

$$X_{TCSC(\alpha)} = \frac{1}{T_{TCSC}}\left(X_{mod} + X_{ref}\right) - X_{TCSC(\alpha)}. \quad (2.28)$$

The TCSC Lead Lag structure with different blocks as gain block, a signal Wash-Out block (as high-pass filter), and two-stage Lead lag blocks. Because TCSC is included in the OHPM model, there are only three new constants [36].

$$K_p = \frac{\partial P_E}{\partial X_{TCSC}}, K_q = \frac{\partial E_q}{\partial X_{TCSC}}, K_v = \frac{\partial V_t}{\partial X_{TCSC}}.$$

The addition of TCSC to AHPM has resulted in the following four new constants:

$$K_p = \frac{\partial T_E}{\partial X_{TCSC}}, K_q = \frac{\partial E'_q}{\partial X_{TCSC}},$$
$$K_d = \frac{\partial E'_d}{\partial X_{TCSC}}, K_{EFD} = \frac{\partial E_{fd}}{\partial X_{TCSC}},$$

2.9 The CPT Model

The OMIBS incorporates both PSS and TCSC in the CPT model. The local oscillation mode can be effectively dampened by the PSS. One generator's rotor oscillation is connected to the rest of the system in this oscillation mode. In the inter-area mode of oscillation there is oscillation of group of SGs of one area with the oscillation of group of SGs of another area. In the CPT model, the TCSC and PSS work together to dampen both local and interarea oscillation modes. Fig. 6 shows the CPT Model.

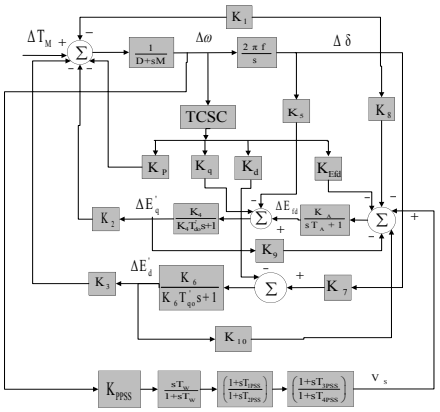

Fig. 6. The CPT Model.

2.9.1 State Space Modelling of CPT with OHPM

$$\begin{bmatrix} \Delta\dot{\delta} \\ \Delta\dot{\omega}_m \\ \Delta\dot{E}'^{q} \\ \Delta\dot{E}_{fd} \end{bmatrix} = \begin{bmatrix} 0 & \omega_B & 0 & 0 \\ -\frac{K_1}{2H} & -\frac{D}{2H} & -\frac{K_2}{2H} & 0 \\ -\frac{K_4}{T'_{d0}} & 0 & -\frac{1}{T'_{d0}K_3} & \frac{1}{T'_{d0}} \\ -\frac{K_A K_5}{T_A} & 0 & -\frac{K_A K_6}{T_A} & -\frac{1}{T_A} \end{bmatrix} \begin{bmatrix} \Delta\delta \\ \Delta\omega_m \\ \Delta E'_q \\ \Delta E_{fd} \end{bmatrix}$$
$$+ \begin{bmatrix} 0 & 0 \\ 0 & -\frac{K_p}{2H} \\ 0 & -\frac{K_q}{T'_{d0}} \\ \frac{K_A}{T_A} & -\frac{K_A K_V}{T_A} \end{bmatrix} \begin{bmatrix} \Delta U_{PSS} \\ \Delta X_{TCSC} \end{bmatrix}.$$

2.9.2 CPT State Space Modelling/ Representation with AHPM

$$\begin{bmatrix} \Delta\dot{\delta} \\ \Delta\dot{\omega}_m \\ \Delta\dot{E}'^{q} \\ \Delta\dot{E}'^{d} \\ \Delta\dot{E}_{fd} \end{bmatrix} = \begin{bmatrix} 0 & \omega_B & 0 & 0 & 0 \\ -\frac{K_1}{2H} & -\frac{D}{2H} & -\frac{K_2}{2H} & -\frac{K_3}{2H} & 0 \\ -\frac{K_5}{T'_{d0}} & 0 & -\frac{1}{T'_{d0}K_4} & 0 & \frac{1}{T'_{d0}} \\ \frac{K_7}{T'_{q0}} & 0 & 0 & -\frac{1}{T'_{q0}K_6} & 0 \\ -\frac{K_A K_8}{T_A} & 0 & -\frac{K_A K_9}{T_A} & -\frac{K_A K_{10}}{T_A} & -\frac{1}{T_A} \end{bmatrix} \begin{bmatrix} \Delta\delta \\ \Delta\omega_m \\ \Delta E'_q \\ \Delta E'_d \\ \Delta E_{fd} \end{bmatrix}$$
$$+ \begin{bmatrix} 0 & 0 \\ 0 & -\frac{K_p}{M} \\ 0 & -\frac{K_q}{T'_{d0}} \\ 0 & -\frac{K_d}{T'_{q0}} \\ \frac{K_A}{T_A} & -\frac{K_A K_{Efd}}{T_A} \end{bmatrix} \begin{bmatrix} \Delta U_{PSS} \\ \Delta X_{TCSC} \end{bmatrix}.$$

3. Problem Formulation and Objective Function

Designing a strong, capable, and efficient system that satisfies the required time domain characteristics, less overshoot in the response of various system parameters and quick oscillation settlement is the objective. The ($\Delta\omega$) is selected as input to the models PSS, TCSC and CPT. The output signals from PSS, TCSC and CPT models are the stabilizing signals and are fed to OMIBS. The oscillations in the system are observed/reflected in the variation/deviation in $(\Delta\omega)$ of SG. Hence the Objective Function (*OF*) considered here is Integral Time Absolute Error (ITAE). The $OF = \int_0^{t_{sim}} |\Delta\omega(t)| dt$ where, t_{sim} is the simulation time. The aim is to minimize the OF with the consideration of different constraints. The other functions are IAE and ISE in which time is not given importance. Hence, ITAE is chosen here. The different constraints are the upper- bound or UB and the lower-bound or LB of the parameters of PSS, TCSC and CPT Models and are given by:

$K_{PPSS}^{MIN} \le K_{PPSS} \le K_{PPSS}^{MAX}$, $T_{1PSS}^{MIN} \le T_{1PSS} \le T_{1PSS}^{MAX}$,
$T_{2PSS}^{MIN} \le T_{2PSS} \le T_{2PSS}^{MAX}$, $T_{3PSS}^{MIN} \le T_{3PSS} \le T_{3PSS}^{MAX}$,
$T_{4PSS}^{MIN} \le T_{4PSS} \le T_{4PSS}^{MAX}$, $K_{PTCSC}^{MIN} \le K_{PTCSC} \le K_{PTCSC}^{MAX}$,
$T_{1TCSC}^{MIN} \le T_{1TCSC} \le T_{1TCSC}^{MAX}$, $T_{2TCSC}^{MIN} \le T_{2TCSC} \le T_{2TCSC}^{MAX}$,
$T_{3TCSC}^{MIN} \le T_{3TCSC} \le T_{3TCSC}^{MAX}$, $T_{4TCSC}^{MIN} \le T_{4TCSC} \le T_{4TCSC}^{MAX}$,
$K_{BTCSC}^{MIN} \le K_{BTCSC} \le K_{BTCSC}^{MAX}$, $T_{1BTCSC}^{MIN} \le T_{1BTCSC} \le T_{1BTCSC}^{MAX}$,
$T_{2BTCSC}^{MIN} \le T_{2BTCSC} \le T_{2BTCSC}^{MAX}$, $T_{3BTCSC}^{MIN} \le T_{3BTCSC} \le T_{3BTCSC}^{MAX}$,
$T_{4BTCSC}^{MIN} \le T_{4BTCSC} \le T_{4BTCSC}^{MAX}$,

4. Snake Optimization Algorithm and Flowcharts

It is a novel and nature-inspired meta-heuristic optimization algorithm proposed in Knowledge-Based Systems in 2022. Snakes are amazing creatures and help in maintaining the ecological balance. The four steps on which the SOA is based are the snake's mating behavior, the source of inspiration, the mathematical modelling and development of the algorithm and finally checking the terminating condition. The algorithm is inspired by the unique mating behavior of snakes. The conditions for mating are the low temperature and the availability of food. If there is no food the snakes search for food or take the existing food. This is related to exploration and exploitation. In the exploitation phase the algorithm searches for the solution in the entire space and in the exploitation phase the algorithm searches the solution around the promising areas. Fig. 7 shows the snake in nature.

Fig. 7. The snake in nature.

4.1 The Pseudo Code of SOA

Step1. Identify the problem parameters such as dimensions, upper and lower bounds,
Step2. Population size, total or maximum number of iterations (T), current iteration (t)
Step3. Randomly initialize the population
Step4. Separate the entire population into two groups
Step5. while $(t \le T)$ do
Step6. Find N_m, N_f from each male and female group
Step7. Find the best male
Step8. Find the best female
Step9. Define the temperature using Eq. (4.4)
Step10. Define the quantity of food using Eq. (4.5)
Step11. If ($Q < 0.25$) then
Step12. Go for exploration phase using Eqs. (4.6), (4.8)
Step13. Else if ($Q > 0.6$) then
Step14. Go for exploitation phase using Eq. (4.10)
Step15. Else If (rand > 0.6) then
Step16. Snakes will be in mode of fighting using Eqs. (4.11)-(4.12)
Step17. else
Step18. Snakes will be in mode of mating using Eqs. (4.15)-(4.16)
Step19. Change the worst female and male using Eqs. (4.19)-(4.20)
Step20. end if
Step21. end if
Step22. end while
Step23. Return the best solution.

4.2 SOA Equations

$$X_i = X_{min} + rx\left(X_{max} - X_{min}\right), \quad (4.1)$$

$$N_m = N/2, \quad (4.2)$$

$$N_f = N - N_m, \quad (4.3)$$

$$\text{Temp} = \text{Exp}\left(\frac{-t}{T}\right), \quad (4.4)$$

$$Q = c_1 \times \exp\left(\frac{t-T}{T}\right), \quad (4.5)$$

$$X_{i,m}(t+1) = X_{rand,m}(t) \pm c_2 \times \left(X_{max} - X_{min}\right) \times rand + X_{min}, \quad (4.6)$$

$$A_m = \exp\left(\frac{-f_{rand,m}}{f_{i,m}}\right), \quad (4.7)$$

$$X_{i,f} = X_{rand,f}(t+1) \pm c_2 A_f \left(\left(X_{max} - X_{min}\right) rand + X_{min}\right), \quad (4.8)$$

$$A_f = \exp\left(\frac{-f_{rand,f}}{f_{i,f}}\right), \quad (4.9)$$

$$X_{i,j}(t+1) = X_{food} \pm c_3 \times Temp \times rand\left(X_{food} - X_{i,j}(t+1)\right), \quad (4.10)$$

$$X_{i,j}(t+1) = X_{i,j}(t) \pm c_3 \times FM \times rand\left(QX_{best,f} - X_{i,j}(t)\right), \quad (4.11)$$

$$X_{i,f}(t+1) = X_{i,f}(t) \pm c_3 \times FF \times rand\left(QX_{best,m} - X_{i,F}(t+1)\right), \quad (4.12)$$

$$FM = \exp\left(\frac{-f_{best,f}}{f_i}\right), \quad (4.13)$$

$$FF = \exp\left(\frac{-f_{best,m}}{f_i}\right), \quad (4.14)$$

$$X_{i,m}(t+1) = X_{i,m}(t) + c_3 \times M_m \times rand\left(QX_{i,f}(t) - X_{i,m}(t)\right), \quad (4.15)$$

$$X_{i,f}(t+1) = X_{i,f}(t) + c_3 \times M_f \times rand\left(QX_{i,m}(t) - X_{i,f}(t)\right), \quad (4.16)$$

$$M_m = \exp\left(\frac{-f_{i,f}}{f_{i,m}}\right), \quad (4.17)$$

$$M_f = \exp\left(\frac{-f_{i,m}}{f_{i,f}}\right), \quad (4.18)$$

$$X_{worst,m} = X_{min}(t) + rand\left(X_{max} - X_{min}\right), \quad (4.19)$$

$$X_{worst,f} = X_{min} + rand\left(X_{max} - X_{min}\right). \quad (4.20)$$

The explanation of these terms for SOA are given in [37].

4.3 The SOA flowchart

Fig. 8 shows the SOA flowchart.

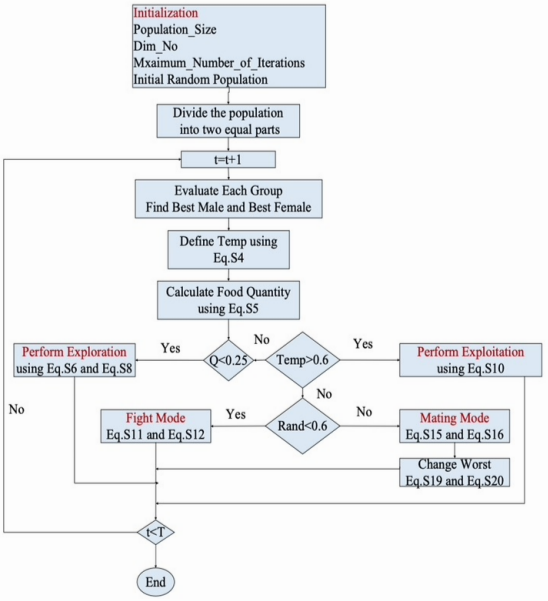

Fig. 8. The SOA Flowchart.

4.4 Testing with the Benchmark functions

The SOA has been checked for 30 benchmark functions obtained from Congress on Evolutionary Computation (CEC) 2017. The three unimodal functions are Rotated and Shifted Bent Cigar Function, Sum of Various Power Functions, and Zakharov functions. There are seven multimodal Functions which are Rotated and Shifted Rosenbrock's, Rastrigin's, Expanded Scaffer's F6, Lunacek -Bi, and Non-Continuous Rastrigin's, Levy, and Schwefel's Functions. There are ten Hybrid Functions and ten Composition Functions. The different statistical results, such as average, minimum and maximum value, median and standard deviation, are compared with different algorithms like Linear Population size reduction-Success-History Adaptation for Differential Evolution(L-SHADE), Moth Flame Optimization (MFO), Harris Hawk Optimizer (HHO), Thermal Exchange

Optimization (TEO), Grasshopper Optimization Algorithm (GOA), Whale Optimization Algorithm (WOA) and SOA. The outcomes demonstrate increased SOA capability and power in relation to these parameters. The statistical results are shown in Table 2. Table 3 shows the plot of functions. The F stands for Function in Table 2.

Table 2. Statistical Results.

F	Algorithm	Avg	Min	Max	Med	STD
F1	L-SHADE	1.14E+10	7.22+E09	1.88+E10	1.04+E10	3.58+E09
	MFO	1.03E+10	1.20+E09	3.23+E10	5.27+E09	9.69+E09
	HHO	3.97E+08	1.87+E08	1.17+E09	3.88+E08	2.46+E08
	TEO	6.23E+10	5.59+E10	7.27+E10	6.33+E10	6.16+E09
	GOA	8.23E+07	3.74+E07	2.63+E08	6.11+E07	6.07+E07
	WOA	5.32E+09	4.20+E09	9.95+E09	5.15+E09	1.71+E09
	SOA	**4.65E+07**	**6.84+E06**	**1.13+E08**	**3.76+E07**	**3.28+E07**
F5	L-SHADE	8.18E+02	7.65E+02	8.73E+02	8.21E+02	3.19E+01
	MFO	6.87E+02	6.41E+02	7.66E+02	6.78E+02	3.31E+01
	HHO	7.68E+02	7.34E+02	8.24E+02	7.77E+02	3.39E+01
	TEO	9.36E+02	9.14E+02	1.00E+03	9.33E+02	3.33E+01
	GOA	6.75E+02	6.30E+02	7.64E+02	6.76E+02	4.42E+01
	WOA	8.57E+02	8.26E+02	9.40E+02	8.52E+02	3.45E+01
	SOA	**6.42E+02**	**5.91E+02**	**7.24E+02**	**6.29E+02**	**3.94E+01**
F13	L-SHADE	1.89E+08	2.44E+07	6.95E+08	1.42E+08	1.67E+08
	MFO	1.50E+08	2.35E+04	2.91E+09	1.21E+05	6.50E+08
	HHO	1.09E+06	7.05E+05	1.81E+06	1.09E+06	3.69E+05
	TEO	2.02E+10	1.78E+10	2.86E+10	2.15E+10	6.18E+09
	GOA	1.22E+05	6.55E+04	2.53E+05	1.07E+05	6.37E+04
	WOA	2.00E+07	3.47E+06	1.73E+08	9.32E+06	3.75E+07
	SOA	**4.17E+04**	**8.10E+03**	**1.36E+05**	**3.84E+04**	**2.79E+04**
F21	L-SHADE	2.60E+03	2.55E+03	2.63E+03	2.60E+03	2.40E+01
	MFO	2.49E+03	2.42E+03	2.56E+03	2.48E+03	4.49E+01
	HHO	2.60E+03	2.55E+03	2.81E+03	2.59E+03	6.49E+01
	TEO	2.82E+03	2.76E+03	2.90E+03	2.84E+03	6.35E+01
	GOA	2.48E+03	2.45E+03	2.58E+03	2.48E+03	3.71E+01
	WOA	2.64E+03	2.57E+03	2.82E+03	2.62E+03	8.83E+01
	SOA	**2.43E+03**	**2.39E+03**	**2.52E+03**	**2.43E+03**	**3.25E+01**

Table 3. Convergence and Box plots of functions.

S.No	F1 Unimodal Function (Shifted and Rotated Bent Cigar Function)	
1	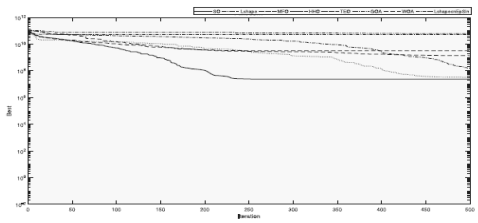	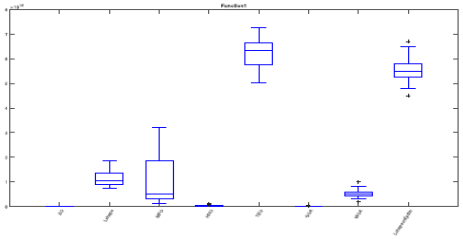
	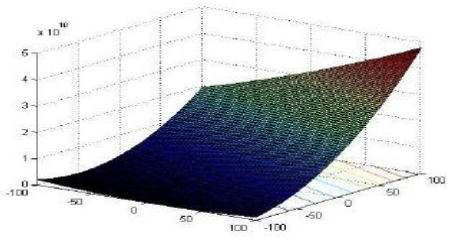	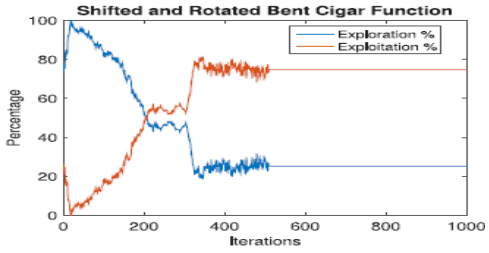

2	F5 Multimodal Function (Shifted and Rotated Rastrigin's Function)

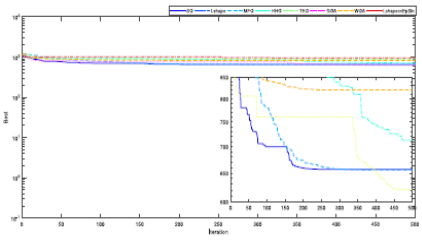

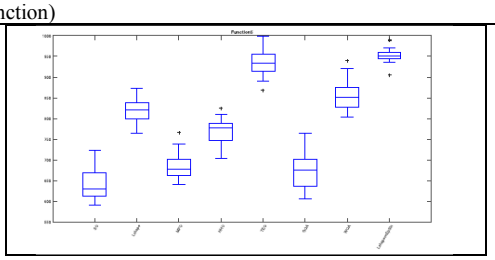

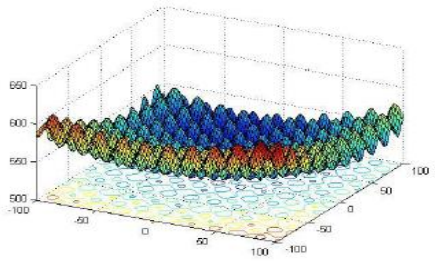

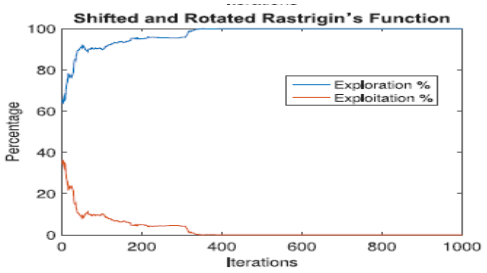

3	F13 Hybrid function 3 N=3

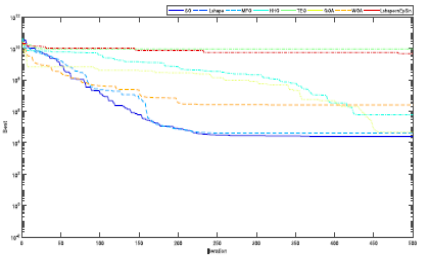

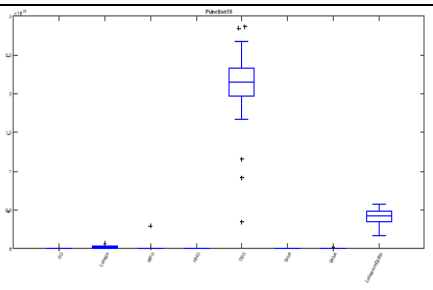

4	F21 Composition Function 1 N=3

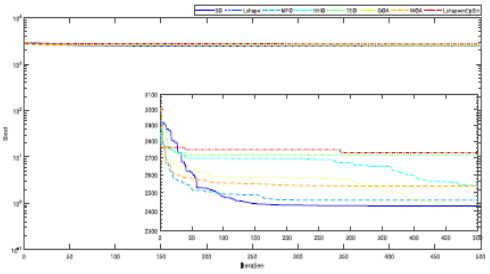

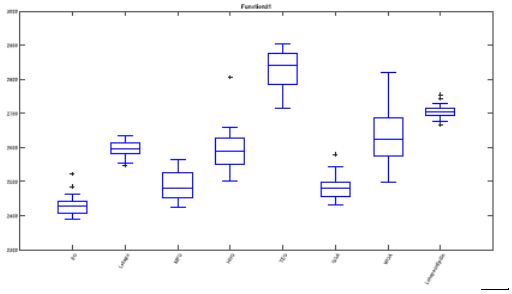

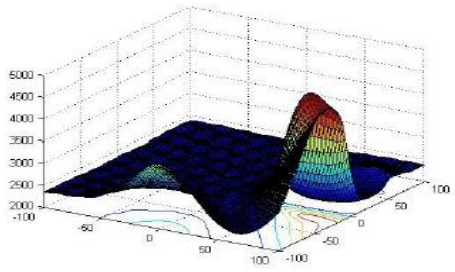

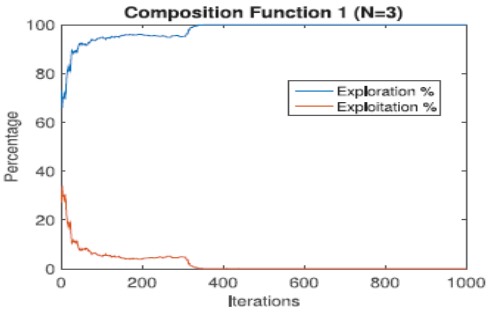

4.5 Various flowcharts

Fig.9 shows the flowchart for PSS with SOA, Fig.10 shows the flowchart for TCSC with SOA. Fig. 11 shows the flowchart for CPT Model with SOA.

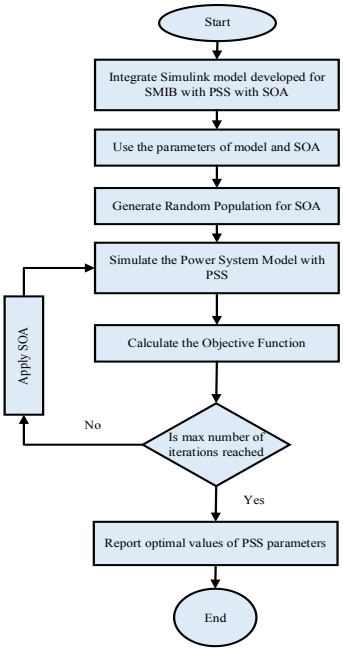

Fig. 9. PSS with SOA.

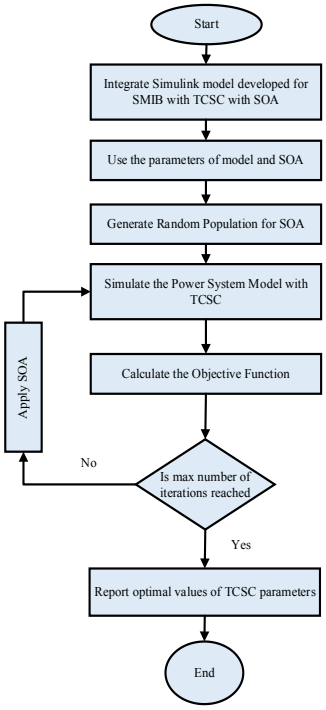

Fig. 10. TCSC with SOA.

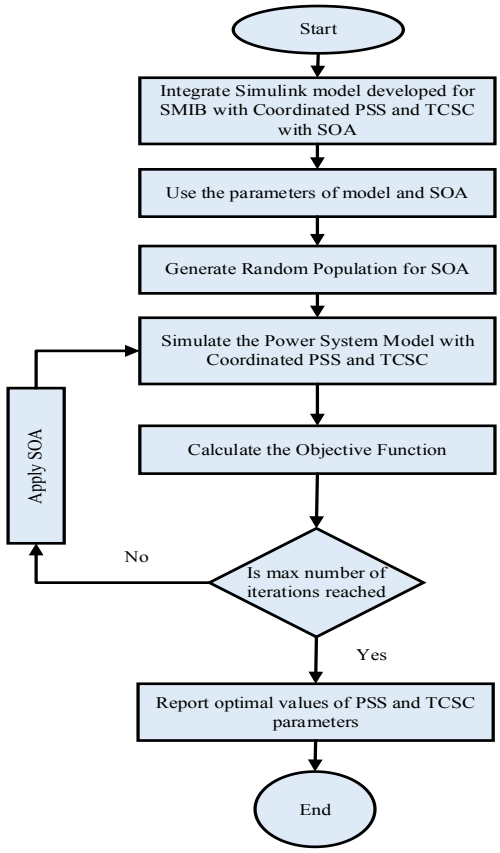

Fig. 11. Coordinated PSS and TCSC Model.

4.6 The parameters of SOA

Table 4 shows the parameters chosen for the models.

Table 4. Parameters of SOA.

Parameter	Value
Population_Size (N)	20
Mxaimum_Number_of_Iterations	50
Dimension (Dim)	10
No of Variables for PSS	5
Upper_Bound_PSS	1.00
Lower_Bound_PSS	0.01
No of Variables for TCSC	5
Upper_Bound_TCSC	1.00
Lower_Bound_TCSC	0.01
No of Variables for CPT	10
Upper_Bound_PSS_TCSC	1.00
Lower_Bound_PSS_TCSC	0.01
Simulation Time	10 seconds
T_W for PSS	10 seconds
T_W for TCSC	10 seconds
T_W for CPT	10 seconds

4.7 The MATLAB simulation model

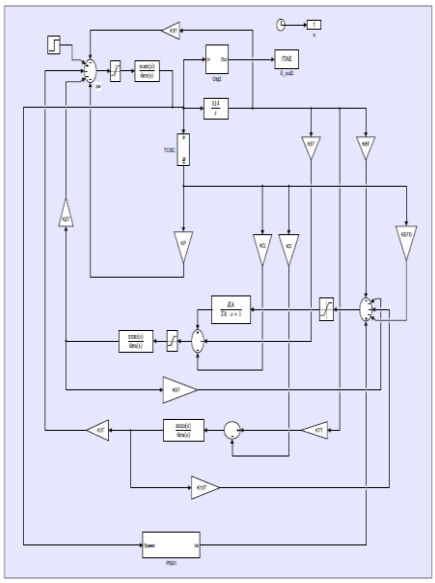

Fig. 12. The Simulation Model.

Fig.12 shows the simulation model from MATLAB. This model has 10 K-Constants.

5. Performance Analysis and Results

The different system parameters are successfully tuned/optimized by SOA. The OF is evaluated for each individual model with the consideration of a (10%) step increase in input i.e., mechanical power at time t = 1.0 second for the loading condition (P = 0.6 p.u. and Q = 0.0224 p.u.). The OF chosen is the minimization in rotor speed. The system's time domain simulation is performed to minimize the OF subject to constraints. It is desired that oscillations should die out fast. Table 5 shows the K-Constants for PSS, TCSC and CPT models. Table 6 shows the gain and time constants of PSS, TCSC and CPT models obtained by SOA. The ITAE error values are given in Table 7. The error is less in the CPT model. The values of 10 K-Constants are determined and fed into the system models PSS, TCSC and CPT.

Table 5. K- Constants.

S. No	Constant	NC	PSS	TCSC	CPT
1	K_1	0.727	0.727	0.801	0.801
2	K_2	1.435	1.435	1.533	1.533
3	K_3	0.318	0.318	0.371	0.371
4	K_4	0.453	0.453	0.424	0.424
5	K_5	1.062	1.062	1.193	1.193
6	K_6	0.759	0.759	0.745	0.745
7	K_7	-0.151	-0.151	-0.163	-0.163
8	K_8	-0.075	-0.075	-0.093	-0.093
9	K_9	0.473	0.473	0.436	0.436
10	K_{10}	-0.253	-0.253	-0.224	-0.224

Table 6. Gain and Time Constants.

S. No	PSS	TCSC	CPT
ITAE	0.0005	0.0004	0.0039

Table 7. The ITAE.

S. No	PSS	TCSC	CPT
1	KPSS=16	KTCSC=4	KBPSS=19
2	T1PSS=0.6988	T1TCSC=0.4404	T1BPSS=0.4169
3	T2PSS=0.4711	T2TCSC=0.5324	T2BPSS=0.3169
4	T3PSS=0.6656	T3TCSC=0.0112	T3BPSS=0.5162
5	T4PSS=0.8455	T4TCSC=0.3207	T4BPSS=0.7511
6			KBTCSC=0.5
7			T1BTCSC=0.1858
8			T2BTCSC=0.5077
9			T3BTCSC=0.3491
10			T4BTCSC=0.3491

5.1 Plot of variation of different parameters.

The response of various parameters for all models is displayed in the various figures below. The open loop model denoted by NC (No Controller) is highly unstable. There is less variation is system parameters with PSS, TCSC and CPT models. The CPT model has the least overshoot and settling time. This reveals the tremendous potential of the proposed SOA in improving the system's damping profile. A robust controller is developed with this excellent SOA and is illustrated by comparing the response curves. The settling time is around 2.0 seconds for various parameters in the CPT model with SOA. This happens due to better mathematical modelling with the higher order SM model 1.1 in AHPM. This shows the better damping capability by this AHPM. The TCSC and CPT models improved the system's power transfer

capacity along with stability and damping profile.

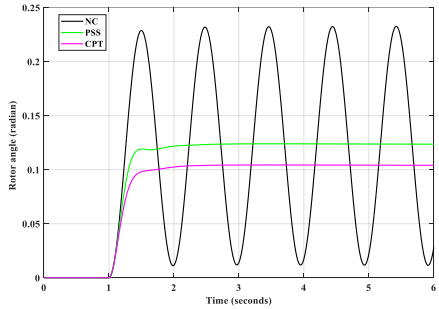

Fig. 13. Rotor Angle.

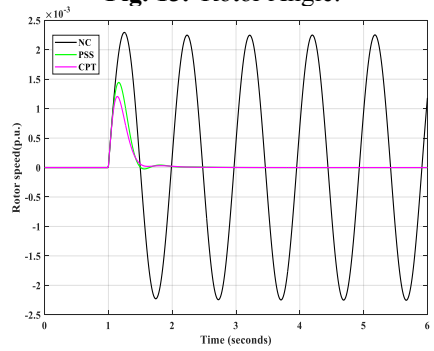

Fig. 14. Rotor Speed.

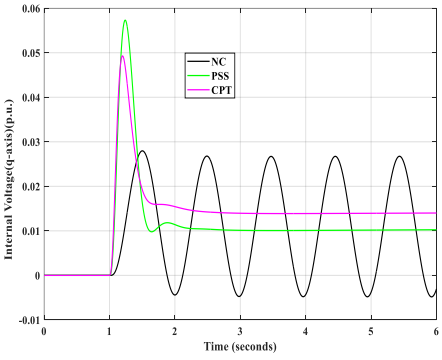

Fig. 15. Internal Voltage.

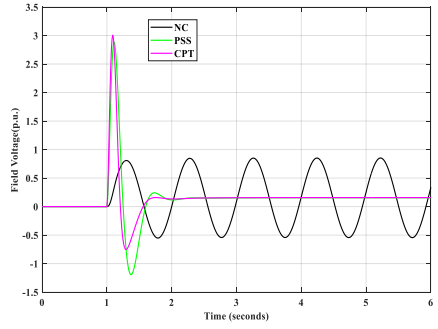

Fig. 16. Field Voltage.

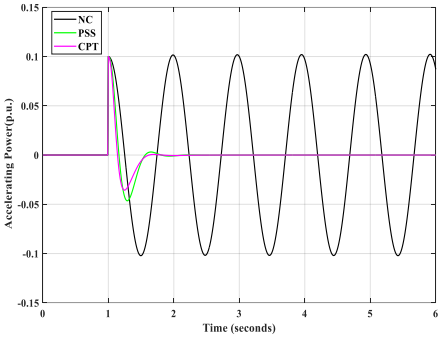

Fig. 17. Accelerating Power.

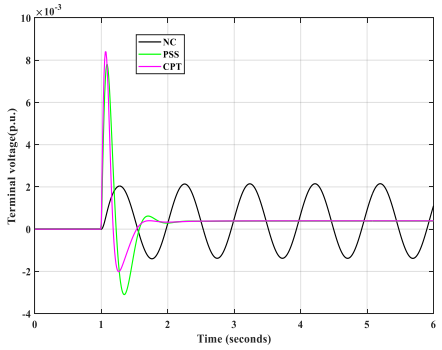

Fig. 18. Terminal Voltage.

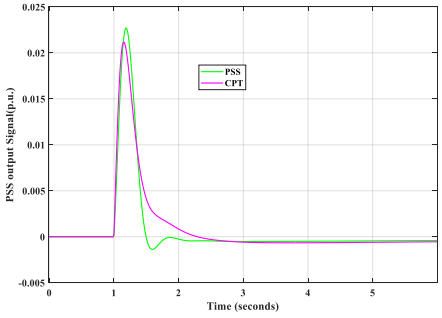

Fig. 19. Stabilizing Signal PSS.

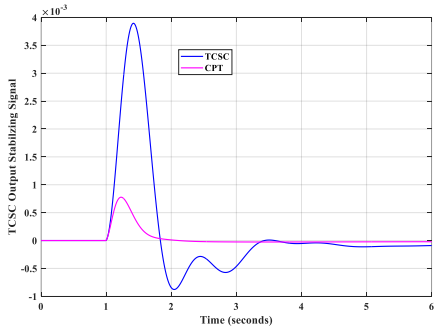

Fig. 20. Stabilizing Signal TCSC.

5.2 System Eigenvalues (EVs) and Damping Ratio (DR)

The EVs are determined for the AHPM without any controller, with PSS, with TCSC, and with CPT. The EV of system A matrix is determined by solving/evaluating the characteristic equation $\det(\lambda I - A) = 0$. The EVs are given by $\lambda_i = \sigma_i \pm j\omega_i$, the DR is given by $\xi_i = -\frac{\sigma_i}{\sqrt{\sigma_i^2 + \omega_i^2}}$ and the frequency of oscillations is given by $f_i = \frac{\omega_i}{2\pi}$.

The real part shows the damping of the system and the imaginary part of complex EV shows the oscillation frequency. The damping ratio should be high and frequency of oscillation should be low for enhanced stability. The EV can be real value or complex value which occur in conjugate pairs. The system EVs and DRs with different models are depicted in Tables 8 and 9.

Table 8. EV and DR with NC and PSS.

S.No/	NC		PSS	
Model	EV	DR	EV	DR
1	0.0012+6.4000i	-1.9400e-04	-14.7000+24.3000i	0.5200
2	0.0012-6.4000i	-1.9400e-04	-14.7000-24.3000i	0.5200
3	-20.3000+27.2000i	0.5990	-5.6500+5.1100i	0.7410
4	-20.3000-27.2000i	0.5990	-5.6500-5.1100i	0.7410
5	-2.6400		-2.3400+0.4710i	0.9800
6			-2.3400-0.4710i	0.9800
7			-0.1020	
8			-1.15	

In Table 8 the EV with NC and PSS models are given. The NC model shows a negative DR (-1.9400e-04) corresponding to EV (0.0012±6.4000i). The DR is improved in the PSS model. In the NC model, the EV (0.0012±6.4000i) is not showing to the left half of the s-plane. This EV has a positive real part showing instability. The highest DR with the PSS model is 98% corresponding to EV (-2.3400±0.4710i). The system shows improvement in stability with the PSS model. The other DRs in this model are 52%, and 74.10% corresponding to different EVs. The DR is shown for only complex conjugate pairs of EV. The EV with purely real numbers is used for showing the location of the EV in the s-plane. The system performance is better with PSS when compared to the NC model.

Table 9. EV and DR with TCSC and CPT.

S.No/	TCSC		CPT	
Model	EV	DR	EV	DR
1	-1.6700+6.4100i	0.2520	-14.9000+22.4000i	0.5530
2	-1.6700-6.4100i	0.2520	-14.9000-22.4000i	0.5530
3	-20.2000+25.7000i	0.6180	-6.3200+7.9000i	0.6240
4	-20.2000-25.7000i	0.6180	-6.3200-7.9000i	0.6240
5	-1.3500+2.5000i	0.4740	-3.7900+0.8690i	0.9750
6	-1.3500-2.5000i	0.4740	-3.7900-0.8690i	0.9750
7	-0.0965		-2.0300+0.241i	0.9930
8	-2.2400		-2.0300-0.241i	0.9930
9			-0.1020	
10			-24.1000	
11			-0.1000	

Table 9 shows the EV with TCSC and CPT models. In the TCSC model, the highest DR obtained is 61.80% corresponding to EV (-20.2000±25.7000i). The highest DR with the CPT model is 99.30% corresponding to EV (-2.0300±0.241i). The highest DR (99.30%) is achieved with the CPT model. The system stability is the best with this model. The other DRs in the CPT model are 55.30%,62.40% 97.50%, corresponding to different EVs. The EV with only the real part (-24.1000) is lying to the left half of the s-plane in the CPT model as compared to the other models. Table 10 shows the dominant EV from all the 4 models. Here, dominant EV is the EV corresponding to the highest DR from each model. The highest DR 99.30% is obtained by the CPT model.

Table 10. Dominant EV and DR.

S. No	Model	Dominant EV	DR	DR (%)
1	NC	-20.3000±27.2000i	0.5990	59.90
2	PSS	-2.3400±0.4710i	0.9800	98.00
3	TCSC	-20.2000±25.7000i	0.6180	61.80
4	CPT	-2.0300±0.241i	0.9930	99.30

5.3 Plot of EV from different models.

Figs. 21-24 show the plot of EVs obtained from MATLAB simulation. The EVs are shifted to left half of s-plane in the CPT model.

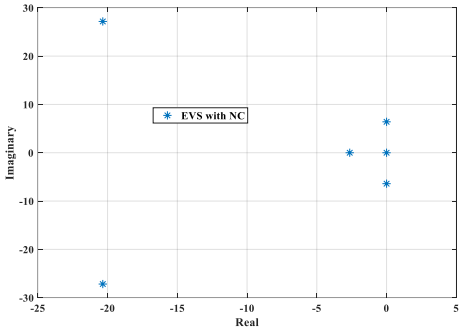

Fig. 21. EV with NC.

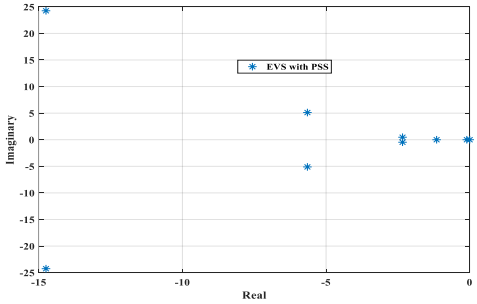

Fig. 22. EV with PSS.

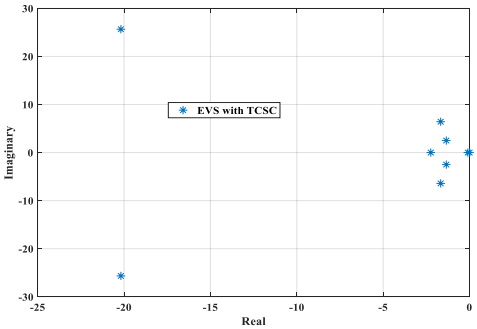

Fig.23. EV with TCSC

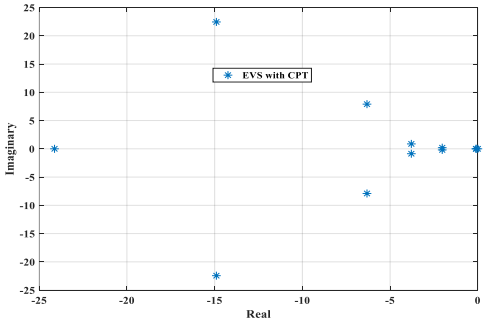

Fig. 24. EV with CPT.

5.4 Plot of convergence

The convergence of SOA with PSS, TCSC and CPT is shown in Figs. 25-27. There is fast convergence with CPT model.

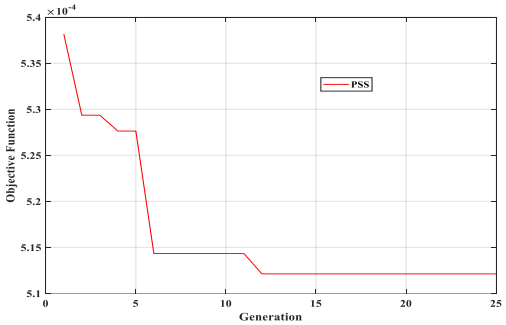

Fig. 25. Convergence PSS.

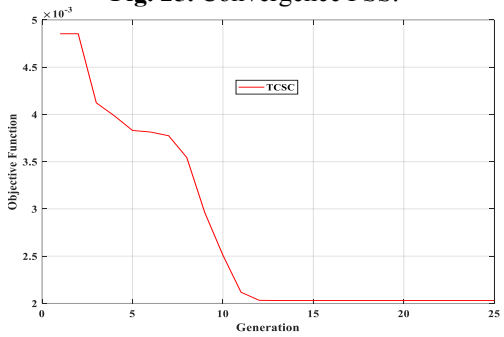

Fig. 26. Convergence TCSC.

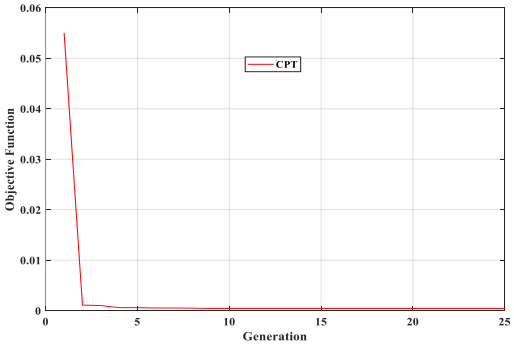

Fig. 27. Convergence CPT.

In the CPT model, the settling time for all parameters is less than two seconds. This time is less than the settling time in references [38-42]. The ITAE is found to be least in the CPT model. This is due to better mathematical modelling of the system with higher order SM Model 1.1 and optimization with SOA. The SOA optimizes the proposed controller parameters successfully. This innovative algorithm achieves a suitable equilibrium between the phases of investigation and exploitation. By comparing the SOA's functionality with benchmark test functions, its capability is certified. Electromechanical

oscillations are significantly suppressed by an AHPM controller. Furthermore, it is demonstrated that the SOA algorithm offers the fastest convergence speed and strongest statistical performance for CPT designs used in SMIB systems.

6. Conclusion

In this manuscript an Advanced Heffron-Phillips Model (AHPM) is developed for designing an effective and efficient power system. This model has 5 state variables instead of 4 state variables in OHPM. This AHPM is developed with the detailed model of SG 1.1 without neglecting the dynamics of d-axis internal voltage. This is the major contribution to this work. The parameters are optimized by a novel SOA which has excellent exploration and exploitation features. Comprehensive simulations and additional eigenvalue analysis are used to realize performance assessments of the outcomes in order to illustrate the efficacy of the SOA. The simulation results demonstrate the high performance of the proposed SOA-based AHPM.

A robust power system is developed with AHPM based on SOA and this is justified by the variation in various parameters. The system eigenval ues are shifted more to the left half of the s-plane which shows improvement in stability. The damping ratio is 99.30 % with the CPT model. The greater the damping ratio, the more stable the system. The settling time for variation in different parameters is less than 2.0 seconds with the CPT model. This demonstrates the enormous potential for improving stability that the suggested AHPM has. Stability in the power system is critical to the nation's technological and economic advancement. This model is capable of meeting the stability challenges even with penetration of renewables in the grid. This is possible with the better mathematical modelling of the system without neglecting any dynamics.

One can expand the work to include multimachine systems. The current goal is to compare stability-related features of the outdated and modern Heffron-Phillips models. Systems for capacitor energy storage (CES) and superconducting magnetic energy storage (SMES) can be used to design the damping controller. CES offers a large storage capacity, while SMES responds quickly to disturbances. It is also possible to use CES and SMES combined. Additional research on battery energy storage systems may also be undertaken.

Acknowledgments

The authors express sincere thanks to the Electrical and Electronics Engineering Department, Principal Ghousia College of Engineering for providing extended support to carry out this work.

References

[1] S. Panda, S. C. Swain, A.K. Baliarsingh ,and C.Ardil." Optimal Supplementary Damping Controller Design for TCSC Employing RCGA. World Academy of Science," Engineering and Technology, International Journal of Electrical and Computer Engineering,2011;11:1600-9.

[2] Sidhartha Panda, "Differential Evolution algorithm for TCSC-based Controller Design", Simulation Modelling Practice and Theory, 2009,17:1618-34.

[3] M.A. Abido, "Pole placement technique for PSS and TCSC-based stabilizer design using simulated annealing, Electrical Power and Energy Systems,2000;22; 543-54.

[4] M.Kashki, Y.L. Abdel-Magid, and M.A. Abido, "Pole-Placement Approach for Robust Optimum Design of PSS and TCSC-Based Stabilizers Using Reinforcement Learning Automata," Springer,2010,383-94.

[5] R. Gandotra, and K. Pal. FACTS Technology: A Comprehensive Review on FACTS Optimal Placement and Application in Power System," Iranian Journal of Electrical and Electronic Engineering,2022; 18(3): 1-14.

[6] Ahmed Hesham, Abd El-Kareem, Mohamed Abd Elhameed, and Mahmoud M. Elkholy, "Effective damping of local low frequency oscillations in power systems integrated with bulk PV generation," Protection and Control of Modern Power Systems,2021; 10:1-16.

[7] Adrian Nocon and Stefan Paszek, "A Comprehensive Review of Power System Stabilizer. Energies," 2023;16:1-32.

[8] Saeed Behzadpoor , Iraj Faraji Davoudkhani Almoataz Youssef Abdelaziz , Zong Woo Geem and Junhee Hong, "Power System Stability Enhancement Using Robust FACTS-Based Stabilizer Designed by a Hybrid Optimization Algorithm," Energies, 2022;15:1-30.

[9] Prabodh Khampariya , Sidhartha Panda , Hisham Alharbi , Almoataz Y. Abdelaziz and Sherif S. M. Ghoneim, "Coordinated Design of Type-2 Fuzzy Lead–Lag-Structured SSSCs and PSSs for Power System Stability Improvement," Sustainability, 2022:14:1-21.

[10] Preeti Ranjan Sahu , Rajesh Kumar Lenka , Rajendra Kumar Khadanga , Prakash Kumar Hota , Sidhartha Panda and Taha Selim Ustun, "Power System Stability Improvement of FACTS Controller and PSS Design: A Time-Delay Approach," Sustainability, 2022; 14:1-23.

[11] S. Kalyani M. Prakash and G. Angeline Ezhilarasi," Transient Stability Studies in SMIB System with Detailed Machine Models," International Conference on Recent Advancements in Electrical, Electronics and Control Engineering,2011:459-64.

[12] Preeti Ranjan Sahu, Prakash Kumar Hota, Sidhartha Panda, Rajesh Kumar Lenka, Sanjeevikumar Padmanaban, and Frede Blaabjerg, "Coordinated design of FACTS controller with PSS for stability enhancement using a novel hybrid Whale Optimization algorithm- Nelder Mead approach," Electric Power Components and Systems, Taylor and Francis Online, 2021;49(16-17):1-28.

[13] Widi Aribowo, "A Novel Improved Sea-Horse Optimizer for Tuning Parameter Power System Stabilizer," Journal of Robotics and Control, 2023;4(1):12-22.

[14] Widi Aribowo, "Golden Jackal Optimization for Parameters Estimation of Photovoltaic Models," Science and Technology Asia,2023;28:198-209.

[15] G.Das, R. Panda, L. Samantaray, and S. Agrawal, "A Novel Non-Entropic Objective Function for Multilevel Optimal Threshold Selection Using Adaptive Equilibrium Optimizer," Iranian Journal of Electrical and Electronic Engineering, 2022;18(2):1-10.

[16] Mohammadreza Jokarzadeh, Mohammad Abedini, and Amir Seifi, "Improving power system damping using a combination of optimal control theory and differential evolution algorithm", ISA Transactions, 2018; 90:169-77.

[17] M. Dodangeh, and N. Ghaffarzadeh, "An Intelligent Machine Learning-Based Protection of AC Microgrids Using Dynamic Mode Decomposition," Iranian Journal of Electrical and Electronic Engineering,2022;4 :1-9.

[18] Kothai Andal C, and Jayapal R, "Improved GA based power and cost management system in a grid-associated PV-wind system," International Journal of Power Electronics and Drive Systems,2021;12(4): 2531-44.

[19] Widi Aribowo, Bambang Suprianto, Unit Three Kartini, and Aditya Prapanca,"Dingo optimization algorithm for designing power system stabilizer," Indonesian Journal of Electrical Engineering and Computer Science,2023; 29(1): 1-7.

[20] Widi Aribowo, Supari Muslim, Bambang Suprianto, and Subuh Isnur Haryudo, Joko, "Tunicate Swarm Algorithm-Neural Network for Adaptive Power System Stabilizer Parameter," Science and Technology, Asia,2021;26(3):50-61.

[21] Javad Morsali, Kazem Zare, and Mehrdad Tarafdar Hagh, "Applying fractional order PID to design TCSC-based damping controller in coordination with automatic generation control of interconnected multi-source power system," Engineering Science and Technology, an International Journal,2017;20(1):1-17.

[22] Javad Morsali Kazem Zare and Mehrdad Tarafdar Hagh, "MGSO optimised TID-based GCSC damping controller in coordination with AGC for diverse-GENCOs multi-DISCOs power system with considering GDB and GRC non-linearity effects," IET Generation, Transmission & Distribution, 2017;11(1):193-208.

[23] Aprajita Salgotra and Somnath Pan, "A frequency domain model-based design of PSS and TCSC controller for damping the small signal oscillations in the power system," International Transactions on Electrical Energy Systems, 2019;29(3):1-10.

[24] Maxwell Martins de Menezes, Percival Bueno de Araujo & Danilo Basseto do Valle, "Design of PSS and TCSC Damping Controller Using Particle Swarm Optimization", Journal of Control, Automation and Electrical Systems, 2016; 27:554-61.

[25] Kazem Zare, Mehrdad Tarafdar Hagh, and Javad Morsali, "Effective oscillation damping of an interconnected multi-source power system with automatic generation control and TCSC," International Journal of Electrical Power & Energy Systems, 2015;65: 220-30.

[26] Mohsen Bakhshi, Mohammad Hosein Holakooie, and Abbas Rabiee, "Fuzzy based damping controller for TCSC using local measurements to enhance transient stability of power systems," International Journal of Electrical Power & Energy Systems, 2017; 85:12-21.

[27] Yonghui Nie, Yidan Zhang, Yan Zhao, Binbin Fang, and Lili Zhang, "Wide-area optimal damping control for power systems based on the ITAE criterion," International Journal of Electrical Power & Energy Systems, 2019,106(4):192-200.

[28] Arnat Watanasungsuit, Noppakun Sangkhiew,Choat Inthawongse, and Peerapop Jomtong, "A Modified AHP for Large-scale MCDM:a Case of Power Station Construction Project Selection," Science and Technology, Asia, 2023,28: 220-30.

[29] Thanwadee Chinda, Rubporn Boonnak, Sakawan Chantabutr, and Suthasinee Rasrungsan," Environmental Perspectives of Electric Vehicles in Thailand: Advantages and Challenges," Science and Technology, Asia,2023;28:88-99.

[30] KR Padiyar, "Power system dynamics stability and control," B.S. Publications, second edition. 2008.

[31] P.R. Gandhi, and S.K. Joshi, "GA and ANFIS based Power System Stabilizer," IEEE,2013:1-7.

[32] P. R. Gandhi, and S. K. Joshi, "Soft Computing Techniques for Designing of Adaptive Power System Stabilizer," IEEE;2019:1-4.

[33] P.R. Gandhi, and S. K. Joshi, "Design of Power System Stabilizer using Genetics Algorithm based Neural Network," International Journal on Electrical Engineering, 2014;14(2):1-13.

[34] Anand Patel, and P. R. Gandhi, "Damping Low Frequency Oscillations using PSO Based Supplementary Controller and TCSC," International Conference on Power Energy, Environment and Intelligent Control, IEEE,2018;38-43.

[35] P.R. Gandhi, and S. K. Joshi, "Smart Control Techniques for design of TCSC and PSS for stability enhancement of dynamical Power System," Applied Soft Computing, Elsevier,2014; C:664-68.

[36] Anand Patel, and P.R. Gandhi, "Damping Oscillations in Detail Model of Synchronous Generator using PSO based PSS," IEEE, 2017:1-6.

[37] Fatma A. Hashim and Abdelazim G. Hussien , "Snake Optimizer: A novel meta-heuristic optimization algorithm," Elsevier, Knowledge-Based Systems,2022;242:1-34.

[38] Hayder Okab Alwan, "A novel approach for coordinated design of TCSC controller and PSS for improving dynamic stability in power systems," Periodicals of Engineering and Natural Sciences ,2023;11(2):102-16.

[39] Sidhartha Panda, and N. P. Padhy, Coordinated Design of TCSC Controller and PSS Employing Particle Swarm Optimization Technique, International Journal of Electrical and Computer Engineering,2007; 1(4):698-706.

[40] Davut İZCİ, "A novel modified arithmetic optimization algorithm for power system stabilizer design," Sigma Journal of Engineering and Natural Sciences,2022; 40(3): 529-41.

[41] Davut Izci, "A novel improved atom search optimization algorithm for designing power system stabilizer," Evolutionary Intelligence,2022;15:2089-103.

[42] Serdar Ekinci, Davut İzci, and Baran Hekimoğlu, "Implementing the Henry Gas Solubility Optimization Algorithm for Optimal Power System Stabilizer Design," Electrica,2021;21(2): 1-9.